Transsynaptic Fish-lips signaling prevents misconnections between nonsynaptic partner olfactory neurons

Qijing Xie[a,b,c,1], Bing Wu[a,b,d,1,2], Jiefu Li[a,b,d], Chuanyun Xu[a,b,d], Hongjie Li[a,b], David J. Luginbuhl[a,b], Xin Wang[a,b], Alex Ward[a,b], and Liqun Luo[a,b,3]

[a]HHMI, Stanford University, Stanford, CA 94305; [b]Department of Biology, Stanford University, Stanford, CA 94305; [c]Neurosciences Graduate Program, Stanford University, Stanford, CA 94305; and [d]Biology Graduate Program, Stanford University, Stanford, CA 94305

Contributed by Liqun Luo, June 21, 2019 (sent for review April 5, 2019; reviewed by Takahiro Chihara and Joris de Wit)

Our understanding of the mechanisms of neural circuit assembly is far from complete. Identification of wiring molecules with novel mechanisms of action will provide insights into how complex and heterogeneous neural circuits assemble during development. In the *Drosophila* olfactory system, 50 classes of olfactory receptor neurons (ORNs) make precise synaptic connections with 50 classes of partner projection neurons (PNs). Here, we performed an RNA interference screen for cell surface molecules and identified the leucine-rich repeat–containing transmembrane protein known as Fish-lips (Fili) as a novel wiring molecule in the assembly of the *Drosophila* olfactory circuit. Fili contributes to the precise axon and dendrite targeting of a small subset of ORN and PN classes, respectively. Cell-type–specific expression and genetic analyses suggest that Fili sends a transsynaptic repulsive signal to neurites of nonpartner classes that prevents their targeting to inappropriate glomeruli in the antennal lobe.

neural connectivity | target selection | *Drosophila* | olfactory system | leucine-rich repeat

The brain comprises extremely complex yet precisely wired neural circuits, which allow animals to faithfully relay and process information. To establish these specific neural connections, a coordinated sequence of developmental steps is taken: Axons and dendrites first navigate to their target zones, then identify the appropriate partners, and finally form functional synapses. Secreted and cell surface–bound factors are required for each of these steps (1–5). These factors can act as either ligands or receptors to allow a developing neurite to sample its environment and select the correct target. Although much progress has been made in both identifying wiring-related molecules and investigating cellular mechanisms underlying each of the steps just described, our understanding of neural circuit assembly is far from complete.

To gain more insight into this developmental process, we studied the *Drosophila* olfactory system. Here, each of the 50 classes of olfactory receptor neurons (ORNs) extend their axons that make synaptic connections with dendrites of their corresponding projection neuron (PN) class in 50 anatomically discrete glomeruli in the antennal lobe (6–8). Because of the stereotyped organization of different synaptic partner pairs, the richness of connections, and the availability of genetic tools, many wiring molecules have been identified and studied in this circuit (9, 10). Furthermore, wiring molecules discovered in this system have guided our understanding of the wiring logic of other neural circuits across different species (11–14).

Here, we designed and carried out an RNA interference (RNAi) screen to identify wiring molecules in a region of the antennal lobe that has not been extensively studied. From this screen, we identified a wiring molecule, Fish-lips (Fili), a leucine-rich repeat–containing transmembrane protein previously known only for its function in regulating dioxin receptor homolog Spineless-mediated apoptosis (15). We investigated the function of Fili in both ORN axon and PN dendrite targeting during olfactory circuit development, and found that Fili signals reciprocally between ORNs and PNs to instruct precise target selection.

Results

A Leucine-Rich Repeat Protein, Fish-Lips, Is Required for the Wiring of Olfactory Neurons. To identify molecules underlying *Drosophila* olfactory-circuit wiring specificity, we previously carried out genetic screens for ORN axon and PN dendrite targeting to the anterior-lateral side of the antennal lobe (11, 16). While certain molecules broadly contribute to the precise wiring of many types of olfactory neurons (17, 18), others have been found to be region- and even glomerulus-specific (9, 11, 16, 19–21). We reasoned that neurons in different locations in the antennal lobe might use a different set of wiring molecules for their circuit assembly. To identify specific PN drivers with reliable expression in other regions of the antennal lobe, we screened a collection of enhancer-GAL4 lines from the FlyLight project (22, 23). We found 5 lines that show robust, specific, and consistent labeling patterns of various PN subtypes (*SI Appendix*, Fig. S1). The labeled glomeruli covered distinct regions, including the dorsolateral, ventromedial, and middle regions of the antennal lobe. We also converted these enhancer-GAL4 lines into a different binary expression system, LexA/LexAop, by fusing each of the specific enhancer fragments to the *LexA* sequence (24). Using 1 of these

Significance

In the fruit fly olfactory system, 50 classes of olfactory receptor neurons (ORNs) make precise synaptic connections with 50 classes of partner projection neurons (PNs). Identification of wiring molecules here can provide general insight into how neural circuits are assembled during development. This paper reports Fish-lips (Fili), a protein spanning the cell membrane, that regulates specific connections in this circuit. We found that some ORN axons are repelled by Fili present on dendrites of nonpartner PNs, preventing them from targeting inappropriate glomeruli. Similarly, some PN dendrites are repelled by Fili expressed by nonpartner ORNs for their correct targeting. These results suggest that Fili mediates repulsion between axons and dendrites of nonsynaptic partners to ensure precise wiring patterns.

Author contributions: Q.X., B.W., and L.L. designed research; Q.X., B.W., C.X., and X.W. performed research; Q.X., B.W., J.L., H.L., D.J.L., and A.W. contributed new reagents/analytic tools; Q.X., B.W., and L.L. analyzed data; and Q.X. and L.L. wrote the paper.

Reviewers: T.C., Hiroshima University; and J.d.W., VIB-KU Leuven Center for Brain & Disease Research.

The authors declare no conflict of interest.

[1]Q.X. and B.W. contributed equally to the work.

[2]Present address: Chan Zuckerberg Biohub, San Francisco, CA 94158.

[3]To whom correspondence may be addressed. Email: lluo@stanford.edu.

This article contains supporting information online at www.pnas.org/lookup/suppl/doi:10.1073/pnas.1905832116/-/DCSupplemental.

Published online July 24, 2019.

lines, *GMR86C10-LexA*, we designed a screening scheme to identify wiring molecules that function in the ventromedial antennal lobe.

Specifically, we used *GMR86C10-LexA > LexAop-mtdT* to label dendrites of VM5v and VM5d PNs, and used *Or98a-mCD8-GFP* and *Or92a-rCD2* to label axons of VM5v and VA2 ORNs, respectively (Fig. 1 *A* and *B*). In addition to these neuronal class–specific markers, we visualized the neuropil using an antibody against *N*-cadherin. Using the panneuronal *C155-GAL4* driver line, we expressed RNAi against predicted transmembrane and secreted molecules. We tested more than 700 RNAi lines (Dataset S1) covering over 200 genes whose protein products contain domain types of leucine-rich repeat (LRR), Ig, cadherin, epidermal growth factor repeat, and fibronectin for their necessity in olfactory neuron–wiring accuracy.

From the screen, we identified several candidates (Dataset S1), including a wiring specificity protein, Fish-lips (Fili). In wild-type animals, *GMR86C10-LexA > LexAop-mtdT* PNs extend their dendrites to only 2 glomeruli—VM5v and VM5d (hereafter VM5 PNs) (Fig. 1*B*). When *fili* was knocked down by either 1 of the 2 independent RNAi lines (i.e., against different regions of *fili*), VM5 PN dendrites ectopically invaded a glomerulus more dorsal and posterior to the correct target (arrowhead in Fig. 1*C* and *SI Appendix*, Fig. S2*A*). Penetrance of the VM5 PN dendrite–targeting phenotype is correlated with *fili* knockdown efficiency (Fig. 1*D* and *SI Appendix*, S2*B*).

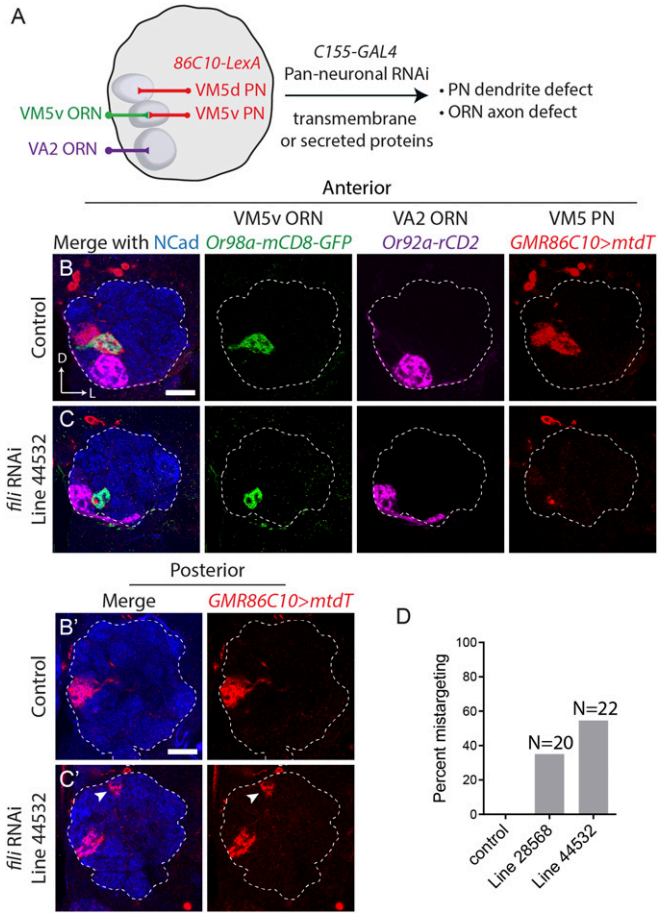

Fig. 1. Identification of Fish-lips as a wiring specificity molecule through an RNAi screen. (*A*) Schematic of RNAi screen. Panneuronal *C155-GAL4* was used to drive *UAS-RNAi* against predicted transmembrane and secreted molecules. Dendrites of 2 PN classes, VM5v and VM5d (hereafter VM5 PNs), are labeled by *GMR86C10-LexA > LexAop-mtdT*. Axons of VM5v and VA2 ORNs are labeled by 2 different markers, *Or98a-mCD8GFP* and *Or92a-rCD2*, respectively. (*B* and *C*) Targeting of dendrites of VM5 PNs (red) and axons of VM5v (green) and VA2 ORNs (magenta) in the antennal lobe on the anterior side. Neuropil staining by the Ncad antibody is shown in blue. Dashed line outlines the antennal lobe neuropil. (*B′* and *C′*) Posterior sections of the same antennal lobes as in *B* and *C*. Dendrites of VM5 PNs and VM5v/VA2 ORN axons target their corresponding glomeruli in control (*B*). *C155-GAL4*–driven *UAS-fili-RNAi* (VDRC 44532) shows PN dendrite–targeting defect (*C*). Ectopic PN targets are indicated by arrowheads on the posterior section of *C′*. (*D*) Quantification of VM5 PN mistargeting of 2 different RNAi lines against *fili* (Bloomington 28568 and VDRC 44532). The phenotype penetrance of 2 independent RNAi lines is 7/20 and 12/22, respectively. (Scale bars, 20 μm.) D, dorsal; L, lateral.

Fili Is Expressed in a Subset of ORNs and PNs. The expression pattern of a wiring molecule can be informative for understanding its mechanism of action. While guidance molecules with a graded expression pattern can be important for the initial coarse targeting of developing neurites (26, 27), wiring molecules with discrete patterning may function to refine the final targeting to a specific region (21). In $fili^{-/-}$ animals, VM5 PN dendrites consistently mistargeted to the same glomerulus. This observation suggests that Fili could serve as a discrete signal for VM5 PN dendrites during their final target selection and refinement.

To assay the expression of Fili, we stained brains at 48 h after puparium formation (48 h APF). At this time, matching between ORN axons and PN dendrites has just been established and the expression pattern likely reflects the molecules used for the final targeting. Additionally, because discrete glomeruli have just formed at this stage, discerning the identity of neurons based on their projection pattern is possible. Immunostaining with Fili antibodies revealed the presence of Fili protein in a subset of glomeruli in the developing antennal lobe (Fig. 3*A*).

Glomerular-specific Fili patterns could be due to Fili's expression in ORNs, PNs, or both. To distinguish between these possibilities, we generated a transcriptional reporter, *fili-GAL4* (28), to study its cell type–specific expression. An artificial exon containing a splicing acceptor, an in-frame *T2A-GAL4*, and a transcription terminator was inserted into a Minos mediated integration cassette (MiMIC) locus (*MI02854*) residing in a coding intron of *fili* (*SI Appendix*, Fig. S5*B*). To validate that this line faithfully represented Fili expression, we crossed it to transgenic flies

Fili encodes a single-pass transmembrane protein that contains 14 LRR motifs in the extracellular domain (*SI Appendix*, Fig. S5*A*). S2 cell transfection experiments validated that the extracellular domain was on the cell surface, as it could be detected by antibody staining without permeabilization (*SI Appendix*, Fig. S3). Fili shares the most amino acid sequence similarities with 2 other LRR proteins, Capricious (Caps) and Tartan (Trn) (15), both of which have been demonstrated to regulate PN dendrite targeting (21). The extracellular domain of Fili is 32% and 30% identical to that of Caps and Trn, respectively (*SI Appendix*, Fig. S4), whereas Caps and Trn are more closely related, sharing 63% identity in their extracellular domains. The intracellular domains are more divergent among these 3 proteins (*SI Appendix*, Fig. S4). The function of Fili in the nervous system has not been reported previously.

To investigate the function of Fili, we generated a null allele using CRISPR-mediated gene editing, which removed the first exon and part of the second exon of *fili* (Fig. 2*A*). According to simple modular architecture research tool (SMART) protein prediction (25), this excision should eliminate the DNA sequence that encodes the start codon, the signal peptide, and more than half of the LRR motifs. We validated this allele by staining brains of $fili^{-/-}$ flies with a Fili antibody we generated against an epitope on the intracellular domain of Fili (*SI Appendix*, Fig. S5*A*). Although the Fili antibody signal was clearly present in heterozygous flies, we detected no signal in $fili^{-/-}$ animals (Fig. 2*C*). Because the targeting epitope of the Fili antibody was not contained in the deleted region, our data suggested that this deletion fully disrupted production of Fili. Similar to the phenotype we observed by panneuronal RNAi knockdown of *fili*, $fili^{-/-}$ animals showed dorsoposterior ectopic targeting of VM5 PN dendrites (Fig. 2*E′* arrowhead).

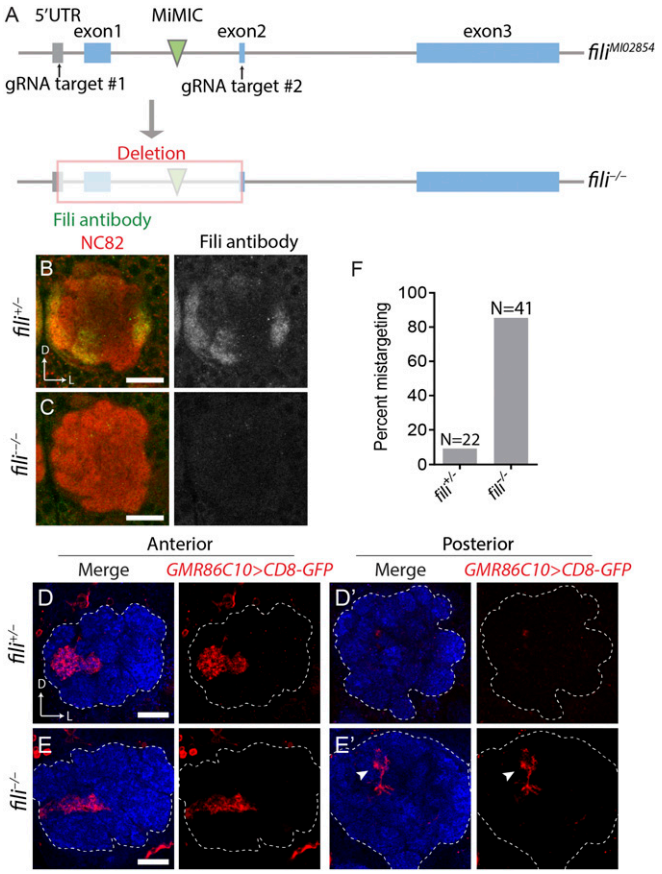

Fig. 2. *fili* mutant recapitulates the RNAi phenotype. (*A*) Schematic of the generation of *fili* null mutant by CRISPR-mediated excision. *vas-Cas9; fili*^{MI02854} eggs were coinjected with 2 gRNAs targeting the 5′ UTR (untranslated region) and the second exon. The first coding exon and part of the second coding exon are deleted in the mutant. Blue bars, coding exons of *fili*. (*B* and *C*) Maximum projection of anti-Fili serum staining (green and gray) of heterozygous control (*B*) and *fili*$^{-/-}$ fly (*C*). (*D* and *E*) Targeting of VM5 PNs labeled by *GMR86C10-GAL4* > *UAS-mCD8GFP* (red) in the antennal lobe of heterozygous *fili*$^{+/-}$ (*D*; mistargeting ratio: 2/22) or homozygous *fili*$^{-/-}$ animals (*E*; mistargeting ratio: 35/41). (*F*) Quantification of mistargeting ratio from *D* and *E*. (Scale bars, 20 μm.)

expressing a membrane fluorescent reporter (*UAS-mCD8-GFP*) and observed a similar GFP pattern compared with the Fili protein pattern in the antennal lobe (*SI Appendix*, Fig. S5*C*). The mCD8-GFP reporter for *fili-GAL4* also showed bright cell body labeling around the antennal lobe not seen in the staining with Fili antibodies. This is likely because the mCD8-GFP reporter did not reflect subcellular localization of the Fili protein.

To visualize the contribution of Fili by ORNs and PNs, we intersected *fili-GAL4* with FLP recombinase lines expressed in either all ORNs (*ey-FLP*) or the majority of PNs (*GH146-FLP*). When combined with *UAS-FRT-STOP-FRT-mCD8GFP*, mCD8-GFP was solely produced in *fili*-positive ORNs or PNs. Using this strategy, we observed that Fili was expressed in ORNs and PNs in a "salt-and-pepper" pattern (Fig. 3 *B* and *D*) reminiscent of the expression of Caps and Trn (11, 21). This expression pattern suggests that Fili likely serves as a discrete determinant that constrains glomerular targeting of neurites instead of setting a gradient for trajectory selection or coarse targeting. Further analysis revealed no statistically significant correlation of *fili* expression between ORNs and PNs (Fisher's exact test, P value = 0.4704). This suggests that Fili likely does not mediate homophilic attraction or repulsion between ORNs and PNs.

Fili in ORNs Signals to VM5 PNs for Proper Dendrite Targeting. To determine which neurons require Fili functions for the proper targeting of VM5 PN dendrites, we carried out mosaic analyses with a repressible cell marker (MARCM) (29) to test a possible cell-autonomous function. Using *hsFLP*-based MARCM, we generated *fili*$^{-/-}$ PN neuroblast clones and observed no mistargeting of VM5 PN dendrites as visualized by *GMR86C10-GAL4* (Fig. 4 *A* and *C*). This indicates that Fili is not required in VM5 PNs for their correct dendrite targeting. In contrast, deleting *fili* in most ORNs using *ey-FLP*–based MARCM combined with a cell-lethal strategy (30) recapitulated the whole-animal *fili*$^{-/-}$ phenotype (Fig. 4 *B* and *C*).

Two mechanisms might account for the above results. First, Fili is required in VM5 ORNs for their correct axon targeting. When those ORN axons mistarget, dendrites of their partner PN classes mistarget with them (16). Second, Fili in ORNs signal to dendrites of VM5 PNs to direct their correct targeting. To test the first possibility, we removed Fili in ORNs and visualized axon targeting of VM5v or VM5d ORNs. We did not observe obvious axon mistargeting (Fig. 4 *D*–*H*). This argues against the first possibility and suggests instead that Fili is expressed by ORNs to signal to VM5 PNs for dendrite target selection. To understand where the Fili signal originates, we checked the expression pattern of Fili in ORNs. We found no Fili expression in VM5v and VM5d ORNs (*SI Appendix*, Fig. S6*A*) at 48 h APF. By contrast, the mistargeted site, DC4, has high *fili* expression in ORNs (*SI Appendix*, Fig. S6 *B* and *C*). This observation suggests that Fili expressed in the ORN class occupying the ectopic target site may repel VM5 PNs to prevent their dendrites from targeting inappropriate glomeruli.

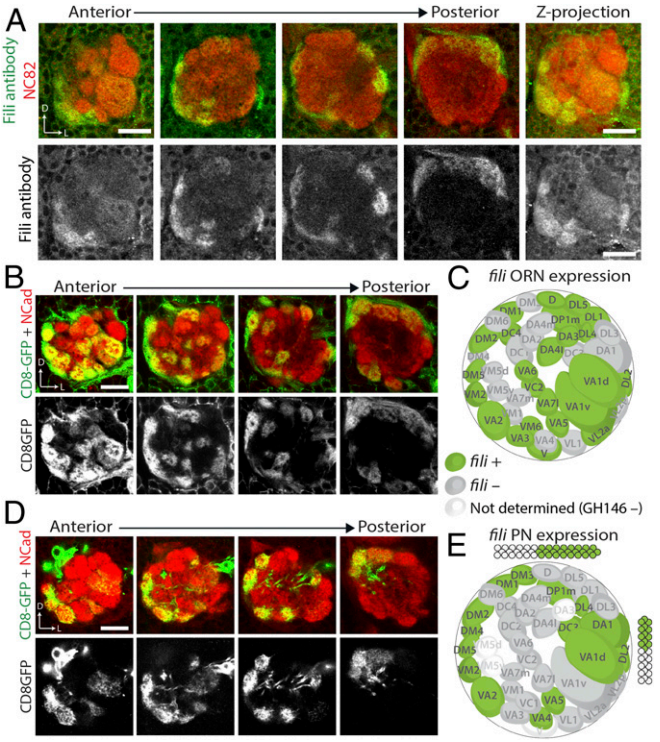

Fig. 3. Fili is differentially expressed in a subset of ORNs and PNs during development. (*A*) anti-Fili serum staining of antennal lobe in wild-type animal (w^{1118}) at 48 h APF (green and gray). Neuropil is stained by the NC82 antibody (red). (*B* and *D*) *ey-FLP* or *GH146-FLP* intersecting with *fili-GAL4* using *UAS-FRT-stop-FRT-mCD8GFP* as a reporter shows *fili* expression pattern in ORNs (*B*) or PNs (*D*) at 48 h APF. (*C* and *E*) Schematic two-dimensional representation of the glomerular innervation pattern of *fili-GAL4*–expressing ORNs (*C*) or PNs (*E*). (Scale bars, 20 μm.)

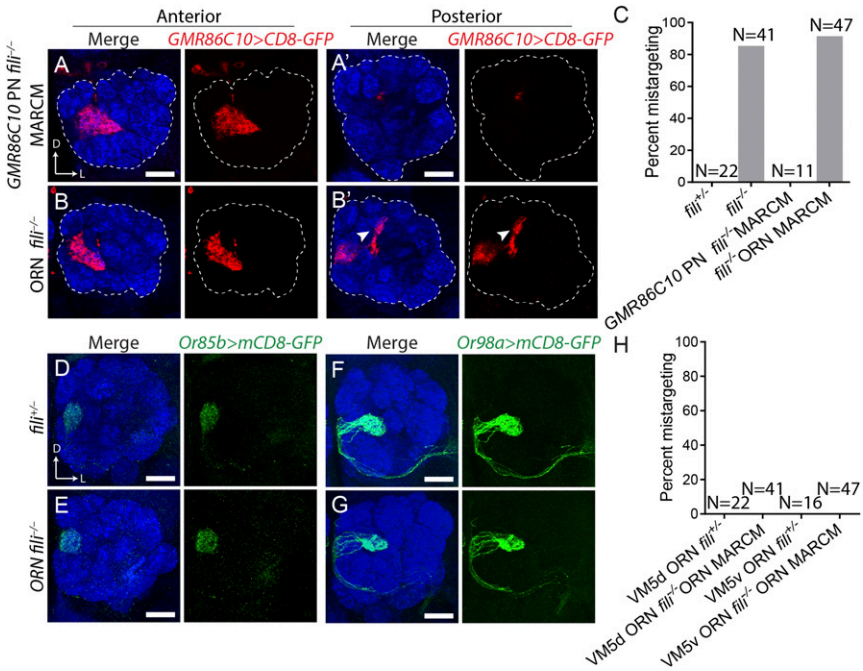

Fig. 4. Fili in ORNs signals to VM5 PNs for the correct targeting of their dendrites. (*A*) Dendrite targeting of *fili*$^{-/-}$ VM5 neuroblast clone produced by *hsFLP* MARCM in a *fili*$^{+/-}$ background (mistargeting in 0/11 antennal lobes). (*B*) Dendrite targeting of *fili*$^{+/-}$ VM5 PNs in animals, with the majority of ORNs being *fili*$^{-/-}$ generated by *ey-FLP* MARCM combined with cell lethal strategy (mistargeting in 43/47 antennal lobes). (*A′* and *B′*) Posterior sections of the same antennal lobe with arrowhead highlighting ectopic targeting of VM5 PN dendrites. (*C*) Quantification of *GMR86C10*+ PN mistargeting from *A* and *B*. (*D* and *E*) Targeting of VM5d ORN axons labeled by *Or85b-GAL4* > *UAS-mCD8GFP* in *fili*$^{+/-}$ animals (mistargeting in 0/22 antennal lobes) (*D*) and in ORN *fili*$^{-/-}$ (mistargeting in 0/41 antennal lobes) (*E*). (*F* and *G*) Targeting of VM5v ORN axons labeled by *Or98a-GAL4* > *UAS-mCD8GFP* in the antennal lobe of *fili*$^{+/-}$ animals (mistargeting in 0/16 antennal lobes) (*F*) and in ORN *fili*$^{-/-}$ animals (mistargeting in 0/47 antennal lobes) (*G*). (*H*) Quantification of mistargeting of VM5d and VM5v ORN axons from *D*–*G*. (Scale bars, 20 μm.)

Fili Is Required for Correct Targeting of a Small Subset of PNs and ORNs. Because Fili is expressed in multiple ORN and PN classes, we examined its involvement in the wiring process of other neuronal classes. Identifying more classes of neurons that require Fili for their targeting allowed us to test whether Fili repels other neurites as a general mechanism of action.

We labeled different ORN and PN classes in a *fili*$^{-/-}$ background to investigate their antennal lobe–targeting fidelity. We examined dendritic targeting of 9 PN classes using 6 drivers and did not observe any obvious targeting defects (*SI Appendix*, Fig. S7). We also labeled 13 different ORN classes in a *fili*$^{-/-}$ background and found three classes with abnormal axon-targeting patterns (*SI Appendix*, Fig. S8). We observed misshapen glomerulus innervated by VA7l ORN axons in *fili*$^{-/-}$ animals (*SI Appendix*, Fig. S8*C*) but no ectopic targeting, which is likely a secondary effect caused by miswiring of other classes of neurons. For both DC1 ORNs and VA1v ORNs, we observed clear ectopic targeting of their axons (*SI Appendix*, Fig. S8 *B* and *D*), indicating that Fili is required for their correct axon target specificity. To better understand how Fili regulates wiring in the context of ORN axon–targeting specificity, we chose to focus on VA1v ORNs as there exists a wealth of tools available to manipulate gene expression in regions adjacent to VA1v.

Fili Is Required in VA1d/DC3 PNs to Prevent Ectopic Targeting of VA1v ORN Axons. In wild-type flies, ORNs of different classes target their axons to distinct glomeruli and never intermingle (Fig. 5*A*). However, in *fili*$^{-/-}$ flies VA1v ORN axons invaded the VA1d glomerulus along with VA1d axons (Fig. 5 *B* and *H*). When we removed *fili* in most ORNs by *ey-FLP*–based MARCM combined with the cell lethal strategy, we did not observe any targeting defect of VA1v ORN axons (Fig. 5 *C* and *H*). Thus, Fili expression in VA1v ORNs (or other ORN classes) is not required for their axon targeting.

We hypothesized that, similar to our observation in *GMR86C10*-positive PNs (Fig. 4), Fili expressed in PNs targeting neighboring glomeruli may repel VA1v ORN axons from targeting inappropriate glomeruli. Our expression analysis using *fili-GAL4* intersected with *GH146-FLP* was consistent with this hypothesis: While VA1v PNs did not express *fili*, neighboring glomeruli VA1d, DC3, and DA1 PNs did (Fig. 5*D*). To more directly test our hypothesis, we generated *fili*$^{-/-}$ neuroblast clones visualized by *Mz19-GAL4* (expressed in DA1 PNs that belong to the lateral neuroblast lineage, and VA1d and DC3 PNs that belong to the anterodorsal neuroblast lineage). At the same time, we labeled VA1d and VA1v ORNs. When the expression of Fili in VA1d/DC3 PNs was eliminated in anterodorsal neuroblast clones, VA1v ORN axons invaded the VA1d glomerulus, similarly to the whole-animal mutant (Fig. 5 *E* and *H*). By contrast, removing *fili* in the lateral neuroblast including DA1 PNs did not cause VA1v ORN axon–targeting defects (Fig. 5*H*).

Because the MARCM strategy generates mutants stochastically, it remained possible that we generated *fili*$^{-/-}$ mutants in other cell types that were not labeled by *Mz19-GAL4* to produce this phenotype. We therefore also used the RNAi strategy to knockdown *fili* in only VA1d and DC3 PNs. To achieve specific GAL4 expression, we utilized the split-GAL4 strategy (31, 32) to generate driver lines specific to VA1d and DC3 PNs. We inserted the hemidriver p65^{AD} component after the last coding exons of C15, a transcription factor that is only expressed by PNs derived from the anterodorsal neuroblast (adPNs) (33), and converted *Mz19-GAL4* to *Mz19-GAL4*^{DBD} using the Homology Assisted CRISPR Knock-in (HACK) strategy (34, 35). When we intersected these 2 components, expression of functional GAL4 was restricted to *Mz19*+ adPNs (VA1d and DC3) (Fig. 5*F*). Using this newly developed driver line, we drove *fili* RNAi in only VA1d and DC3 PNs, and found that this manipulation recapitulated VA1d mistargeting for VA1v ORN axons as observed in *fili*$^{-/-}$ mutants (Fig. 5 *G* and *H*). Moreover, VA1v ORN axons did not invade the DC3 glomerulus when Fili was removed from VA1d and DC3 PNs by MARCM or RNAi. Thus, analogous to VM5 PNs, expression of Fili on the synaptic partner corresponding to the ectopic targeting site is critical for correct axon targeting of VA1v ORN axons. Together, these results suggest that Fili repels neurites of the nonmatching synaptic partner class to restrict them to the correct target.

Discussion

Here, we developed an assay for identifying wiring molecules in the ventromedial region of the *Drosophila* antennal lobe. Through an RNAi screen for cell surface molecules, we discovered that Fili,

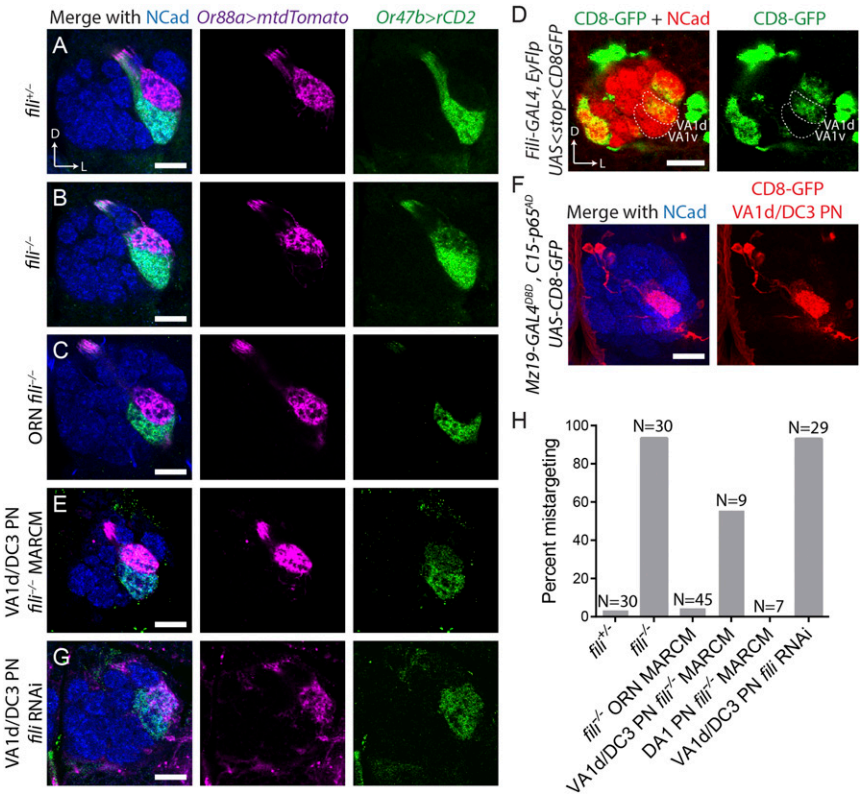

Fig. 5. Fili in VA1d/DC3 PNs prevents ectopic targeting of VA1v ORN axons to VA1d glomerulus. (*A*) VA1d and VA1v ORNs labeled by *Or88a-mTdT* (magenta) and *Or47b-rCD2* (green), respectively, target their axons to 2 neighboring glomeruli in a stereotyped manner in $fili^{+/-}$ animals (mistargeting in 2/30 antennal lobes). (*B*) In $fili^{-/-}$ animals, VA1v ORN axons invade VA1d glomerulus (mistargeting in 29/31 antennal lobes). (*C*) Deletion of *fili* in most ORNs using *ey-FLP* MARCM combined with cell lethal strategy does not alter VA1v ORN axon targeting (mistargeting in 2/45 antennal lobes). (*D*) Expression of Fili in VA1v and VA1d PNs, shown by CD8-GFP (green) using intersection between *GH146-FLP* and *fili-GAL4*. The corresponding glomeruli are outlined by dashed line. (*E*) Deletion of Fili in anterodorsal neuroblast clones (which include VA1d PNs) using *Mz19-GAL4 hsFLP* MARCM causes VA1v ORN axons to mistarget to VA1d glomerulus (mistargeting in 5/9 antennal lobes). (*F*) $Mz19\text{-}GAL4^{DBD}$, $C15\text{-}p65^{AD}$ produces functional GAL4 in only VA1d/DC3 PNs to drive *UAS-mCD8-GFP* expression (red). Maximum z-projection is shown. (*G*) $Mz19\text{-}GAL4^{DBD}$, $C15\text{-}p65^{AD}$ drives *UAS-fili-RNAi* (VDRC 44532), causing VA1v ORN axons to mistarget to VA1d glomerulus (mistargeting in 27/29 antennal lobes). (*H*) Quantification of VA1v ORN axon mistargeting from *A*, *C*, *E*, and *G*. (Scale bars, 20 μm.)

an LRR-containing transmembrane protein, participates in the assembly of the *Drosophila* olfactory circuit. Detailed expression and genetic analyses suggest that Fili acts as a repellent in ORNs for PNs, and in PNs for ORNs, to prevent invasion of neurites into inappropriate glomeruli.

Before this study, Fili had been implicated in cell–cell interaction in the detection of misspecified cells in the wing disk (15). Apoptosis induced by ectopic expression of *Spineless* is regulated by Fili expression. Along with Caps and Trn (36), Fili appears to participate in short-range cell interaction to support cell survival in the wing disk. In the nervous system, LRR-containing proteins have been widely implicated in neural circuit assembly (37). The unique curved structure of LRR combined with exposed β-sheets on the concave side makes LRR an effective protein-binding motif (38). Furthermore, different LRRs form distinct structures, permitting interaction with a diverse collection of proteins (39, 40). These unique binding characteristics enable secreted or membrane-associated LRR proteins to play central roles in diverse aspects of nervous system development and function.

Our results suggest that Fili sends a transsynaptic repulsive signal between ORNs and PNs. Although some LRRs are shown to have binding affinity to themselves (41–44), we note that some glomeruli are innervated by both Fili-positive ORN axons and PN dendrites (Fig. 3 *C* and *E*), arguing against a homotypic mechanism for Fili-mediated repulsion. A more probable explanation is that neurons that require Fili for their targeting specificity express a receptor for Fili and are thus repelled by regions with high Fili expression. Future identification of the Fili receptor will substantiate this hypothesis. Since VA1v ORNs express both Fili and the presumed Fili receptor, Fili does not appear to mediate ORN–ORN repulsion.

Despite Fili's expression in many classes of ORNs and PNs, we observed that only a small fraction of these classes requires Fili for correct axon or dendrite targeting. The sparsity of neurons that manifest observable wiring defects in Fili mutants might be explained by the hypothesis that neurons use a combinatorial and redundant coding strategy to specify their connections (9). As we observed previously, a typical ORN or PN class uses multiple molecules for their axon or dendrite targeting. Our recent single-cell RNAseq data of both PNs and ORNs revealed that the cell surface landscape between different classes of PNs and ORNs is usually distinguished by multiple molecules (33, 45). Therefore, when a single wiring molecule is perturbed, the cell surface landscape may still resemble the original neuronal class more closely than other classes, thus permitting correct neurite targeting for many neurons. A more comprehensive understanding of the overarching wiring strategies of this circuit will benefit from simultaneous manipulation of multiple wiring molecules that cooperate in specifying the connectivity within individual neuronal classes.

Materials and Methods

Immunostaining. *Drosophila* brain dissection and immunostaining were performed according to previously described methods (46). Primary antibodies used in this study included rat anti-Ncad [N-Ex #8; 1:40; Developmental Studies Hybridoma Bank (DSHB)], chicken anti-GFP (1:1,000; Aves Labs), rabbit anti-DsRed (1:500; Clontech), mouse anti-rCD2 (OX-34; 1:200; AbD Serotec), mouse nc82 (1:35; DSHB), anti-HRP conjugated with Cy5 (1:200; Jackson ImmunoResearch), and rat anti-Fili (1:200; custom produced by Thermo Fisher Scientific against a peptide epitope containing Fili residues 684 to 701 DDEPEHLYERFDHYEYPD). Fili antibody was preabsorbed by $fili^{-/-}$ larval brains to remove nonspecific binding. Secondary antibodies raised in goat or donkey against rabbit, mouse, rat, and chicken antisera were used, conjugated to Alexa 405, FITC, 568, or 647 (Jackson ImmunoResearch). Confocal images were collected with a Zeiss LSM 780 and processed with Zen software and ImageJ.

S2 Cell Staining. The S2 cell–staining protocol was adapted from a previously described method (47). We generated *pUAST-attB-Fili* from cDNA and then performed 2 rounds of mutagenesis to insert V5 and FLAG tags. The final construct, *UAS-SP-V5-Fili-FLAG*, contained a V5 tag directly after the signal peptide of Fili and a 3XFLAG tag right before the stop codon. S2 cells were cotransfected with *Actin-GAL4* and *UAS-SP-V5-Fili-FLAG* plasmids or only with *Actin-GAL4* plasmid as a negative control. After 48 h, transfected cells were incubated with rabbit anti-V5 antibody (1:200; GeneScript) and mouse anti-FLAG M2 antibody (1:200; Sigma-Aldrich) either before

(nonpermeabilized condition) or after (permeabilized condition) 4% PFA fixation and permeabilization with 0.3% Triton in PBS. Cells were then washed with PBS, incubated with secondary antibodies, and imaged.

RNAi Screening. The RNAi screen fly was generated as follows: *C155-GAL4* was recombined with *UAS-dcr2* on the X chromosome. *GMR86C10-LexA*, *LexAop-mtdT*, *Or98a-mCD8GFP*, and *Or92a-rCD2* were recombined and located on the second chromosome. *UAS-RNAi* males were crossed to this screening line, and the resulting flies were kept at 25 °C for 2 d after egg laying and then transferred to 29 °C to enhance the GAL4/UAS expression system.

Generation of *fili* Mutant. We generated 2 gRNA constructs using the BbsI-chiRNA plasmid (48). One gRNA contained a targeting site 5′ to the start codon of *fili* and one 3′ to the start of the second coding exon. These 2 gRNA constructs were coinjected into *Drosophila* embryos with *vas-cas9*, a *yellow* gene (*y*) mutant allele on the X chromosome, and MI02854 containing an exogenous *y* gene on the second chromosome. G_0 flies were crossed to balancer flies and individuals in the F_1 generation were selected for loss of *y*. Successful events were balanced and confirmed by sequencing.

Mosaic Analysis. The *hsFLP* MARCM analyses were performed as previously described (29, 49) with slight modifications. *GMR86C10-GAL4* was used for labeling VM5 PNs, and *Mz19-GAL4* was used for labeling VA1d, DC3, and DA1 PNs in adult-stage *Drosophila*. Larvae (24 to 48 h after hatching) were heat-shocked for 1 h to obtain neuroblast clones.

Transgene Generation. To generate enhancer-LexA lines labeling different PNs, including *GMR86C10-LexA*, gateway vector–containing enhancer sequences (23) were recombined into the *pBPnlsLexAp65Uw* vector (32) through LR reaction (Invitrogen) and the resulting constructs were injected into *attP2* and *attP40* landing sites by integrase-mediated transgenesis. *Or92a-rCD2* was made by cloning the rat CD2 coding region (50) downstream of the Or92a promoter sequence, and a transgenic animal was made through P-element transformation (51). *C15-p65^{AD}* was generated by coinjecting a gRNA (cloned in pU6-BbsI-chiRNA) targeting the end of the last exon and donor sequence containing homology arms *p65(AD)::Zip+* and *3XP3-RFP-SV40* (31). *Mz19-Gal4^{DBD}* was generated using the HACK strategy (35). We replaced the QF2 sequence of *pBPGUw-HACK-G4 > QF2* with the DNA-binding domain of GAL4 cloned from *pBS-KS-attB2-SA(0)-T2A-Gal4DBD-Hsp70 polyA*, and injected it into *Mz19-GAL4; vas-Cas9* embryos.

ACKNOWLEDGMENTS. We thank G. Rubin, H. Bellen, T. Lee, the Vienna Stock Center, the Bloomington Stock Center, the *Drosophila* Genomics Resource Center, and Addgene for reagents. We thank T. Li, C.N. McLaughlin, A. Shuster, J. Ren, J. Lui, and D. Pederick for helpful discussions and comments on the manuscript. This work was supported by NIH Grant R01 DC005982 (to L.L.). L.L. is a Howard Hughes Medical Institute investigator.

1. J. R. Sanes, M. Yamagata, Many paths to synaptic specificity. *Annu. Rev. Cell Dev. Biol.* **25**, 161–195 (2009).
2. S. Yogev, K. Shen, Cellular and molecular mechanisms of synaptic specificity. *Annu. Rev. Cell Dev. Biol.* **30**, 417–437 (2014).
3. Y.-N. Jan, L. Y. Jan, Branching out: Mechanisms of dendritic arborization. *Nat. Rev. Neurosci.* **11**, 316–328 (2010).
4. T. C. Südhof, Towards an understanding of synapse formation. *Neuron* **100**, 276–293 (2018).
5. A. L. Kolodkin, M. Tessier-Lavigne, Mechanisms and molecules of neuronal wiring: A primer. *Cold Spring Harb. Perspect. Biol.* **3**, a001727 (2011).
6. L. B. Vosshall, R. F. Stocker, Molecular architecture of smell and taste in *Drosophila*. *Annu. Rev. Neurosci.* **30**, 505–533 (2007).
7. C.-Y. Su, K. Menuz, J. R. Carlson, Olfactory perception: Receptors, cells, and circuits. *Cell* **139**, 45–59 (2009).
8. R. I. Wilson, Early olfactory processing in *Drosophila*: Mechanisms and principles. *Annu. Rev. Neurosci.* **36**, 217–241 (2013).
9. W. Hong, L. Luo, Genetic control of wiring specificity in the fly olfactory system. *Genetics* **196**, 17–29 (2014).
10. H. Li, S. A. Shuster, J. Li, L. Luo, Linking neuronal lineage and wiring specificity. *Neural Dev.* **13**, 5 (2018).
11. W. Hong, T. J. Mosca, L. Luo, Teneurins instruct synaptic partner matching in an olfactory map. *Nature* **484**, 201–207 (2012).
12. T. J. Mosca, W. Hong, V. S. Dani, V. Favaloro, L. Luo, Trans-synaptic Teneurin signalling in neuromuscular synapse organization and target choice. *Nature* **484**, 237–241 (2012).
13. P. Antinucci, N. Nikolaou, M. P. Meyer, R. Hindges, Teneurin-3 specifies morphological and functional connectivity of retinal ganglion cells in the vertebrate visual system. *Cell Rep.* **5**, 582–592 (2013).
14. D. S. Berns, L. A. DeNardo, D. T. Pederick, L. Luo, Teneurin-3 controls topographic circuit assembly in the hippocampus. *Nature* **554**, 328–333 (2018).
15. T. Adachi-Yamada *et al*., Wing-to-leg homeosis by Spineless causes apoptosis regulated by Fish-lips, a novel leucine-rich repeat transmembrane protein. *Mol. Cell. Biol.* **25**, 3140–3150 (2005).
16. A. Ward, W. Hong, V. Favaloro, L. Luo, Toll receptors instruct axon and dendrite targeting and participate in synaptic partner matching in a *Drosophila* olfactory circuit. *Neuron* **85**, 1013–1028 (2015).
17. H. Zhu, L. Luo, Diverse functions of N-cadherin in dendritic and axonal terminal arborization of olfactory projection neurons. *Neuron* **42**, 63–75 (2004).
18. H. Zhu *et al*., Dendritic patterning by Dscam and synaptic partner matching in the *Drosophila* antennal lobe. *Nat. Neurosci.* **9**, 349–355 (2006).
19. W. J. Joo, L. B. Sweeney, L. Liang, L. Luo, Linking cell fate, trajectory choice, and target selection: Genetic analysis of sema-2b in olfactory axon targeting. *Neuron* **78**, 673–686 (2013).
20. J. Li *et al*., Stepwise wiring of the *Drosophila* olfactory map requires specific Plexin B levels. *eLife* **7**, e39088 (2018).
21. W. Hong *et al*., Leucine-rich repeat transmembrane proteins instruct discrete dendrite targeting in an olfactory map. *Nat. Neurosci.* **12**, 1542–1550 (2009).
22. A. Jenett *et al*., A GAL4-driver line resource for *Drosophila* neurobiology. *Cell Rep.* **2**, 991–1001 (2012).
23. B. D. Pfeiffer *et al*., Tools for neuroanatomy and neurogenetics in *Drosophila*. *Proc. Natl. Acad. Sci. U.S.A.* **105**, 9715–9720 (2008).
24. S. L. Lai, T. Lee, Genetic mosaic with dual binary transcriptional systems in *Drosophila*. *Nat. Neurosci.* **9**, 703–709 (2006).
25. J. Schultz, F. Milpetz, P. Bork, C. P. Ponting, SMART, a simple modular architecture research tool: Identification of signaling domains. *Proc. Natl. Acad. Sci. U.S.A.* **95**, 5857–5864 (1998).
26. T. Komiyama, L. B. Sweeney, O. Schuldiner, K. C. Garcia, L. Luo, Graded expression of semaphorin-1a cell-autonomously directs dendritic targeting of olfactory projection neurons. *Cell* **128**, 399–410 (2007).
27. T. Imai, M. Suzuki, H. Sakano, Odorant receptor-derived cAMP signals direct axonal targeting. *Science* **314**, 657–661 (2006).
28. F. Diao *et al*., Plug-and-play genetic access to *Drosophila* cell types using exchangeable exon cassettes. *Cell Rep.* **10**, 1410–1421 (2015).
29. T. Lee, L. Luo, Mosaic analysis with a repressible cell marker for studies of gene function in neuronal morphogenesis. *Neuron* **22**, 451–461 (1999).
30. T. P. Newsome, B. Asling, B. J. Dickson, Analysis of *Drosophila* photoreceptor axon guidance in eye-specific mosaics. *Development* **127**, 851–860 (2000).
31. H. Luan, N. C. Peabody, C. R. Vinson, B. H. White, Refined spatial manipulation of neuronal function by combinatorial restriction of transgene expression. *Neuron* **52**, 425–436 (2006).
32. B. D. Pfeiffer *et al*., Refinement of tools for targeted gene expression in *Drosophila*. *Genetics* **186**, 735–755 (2010).
33. H. Li *et al*., Classifying *Drosophila* olfactory projection neuron subtypes by single-cell RNA sequencing. *Cell* **171**, 1206–1220.e22 (2017).
34. C.-C. Lin, C. J. Potter, Editing transgenic DNA components by inducible gene replacement in *Drosophila melanogaster*. *Genetics* **203**, 1613–1628 (2016).
35. T. Xie *et al*., A genetic toolkit for dissecting dopamine circuit function in *Drosophila*. *Cell Rep.* **23**, 652–665 (2018).
36. M. Milán, L. Pérez, S. M. Cohen, Short-range cell interactions and cell survival in the Drosophila wing. *Dev. Cell* **2**, 797–805 (2002).
37. J. de Wit, W. Hong, L. Luo, A. Ghosh, Role of leucine-rich repeat proteins in the development and function of neural circuits. *Annu. Rev. Cell Dev. Biol.* **27**, 697–729 (2011).
38. B. Kobe, A. V. Kajava, The leucine-rich repeat as a protein recognition motif. *Curr. Opin. Struct. Biol.* **11**, 725–732 (2001).
39. S. G. Buchanan, N. J. Gay, Structural and functional diversity in the leucine-rich repeat family of proteins. *Prog. Biophys. Mol. Biol.* **65**, 1–44 (1996).
40. J. Bella, K. L. Hindle, P. A. McEwan, S. C. Lovell, The leucine-rich repeat structure. *Cell. Mol. Life Sci.* **65**, 2307–2333 (2008).
41. A. Nose, V. B. Mahajan, C. S. Goodman, Connectin: A homophilic cell adhesion molecule expressed on a subset of muscles and the motoneurons that innervate them in *Drosophila*. *Cell* **70**, 553–567 (1992).
42. D. E. Krantz, S. L. Zipursky, *Drosophila* chaoptin, a member of the leucine-rich repeat family, is a photoreceptor cell-specific adhesion molecule. *EMBO J.* **9**, 1969–1977 (1990).
43. J. A. Howitt, N. J. Clout, E. Hohenester, Binding site for Robo receptors revealed by dissection of the leucine-rich repeat region of Slit. *EMBO J.* **23**, 4406–4412 (2004).
44. E. Özkan *et al*., An extracellular interactome of immunoglobulin and LRR proteins reveals receptor-ligand networks. *Cell* **154**, 228–239 (2013).
45. H. Li *et al*., Coordinating receptor expression and wiring specificity in olfactory receptor neurons. bioRxiv:10.1101/594895 (31 March 2019).
46. J. S. Wu, L. Luo, A protocol for dissecting *Drosophila melanogaster* brains for live imaging or immunostaining. *Nat. Protoc.* **1**, 2110–2115 (2006).
47. W. Zhang *et al*., Ankyrin repeats convey force to gate the NOMPC mechanotransduction channel. *Cell* **162**, 1391–1403 (2015).
48. S. J. Gratz, J. Wildonger, M. M. Harrison, K. M. O'Connor-Giles, CRISPR/Cas9-mediated genome engineering and the promise of designer flies on demand. *Fly (Austin)* **7**, 249–255 (2013).
49. J. S. Wu, L. Luo, A protocol for mosaic analysis with a repressible cell marker (MARCM) in *Drosophila*. *Nat. Protoc.* **1**, 2583–2589 (2006).
50. O. M. Dunin-Borkowski, N. H. Brown, Mammalian CD2 is an effective heterologous marker of the cell surface in *Drosophila*. *Dev. Biol.* **168**, 689–693 (1995).
51. E. Fishilevich, L. B. Vosshall, Genetic and functional subdivision of the *Drosophila* antennal lobe. *Curr. Biol.* **15**, 1548–1553 (2005).